Thrust Density Enhancement by Increasing Propellant Mass-Flux in an Electrostatic-Magnetic Hybrid Thruster

Daisuke Ichihara,[1] Koichiro Oka[2], Ayumi Higo[2], Yusuke Nakamura[1], Kiyoshi Kinefuchi[3] and Akihiro Sasoh[4]
Nagoya University, Nagoya 464-8603, Japan

Nomenclature

B = magnetic field strength, T

e = elementary charge, C

F = thrust, N

g = gravitational acceleration, m/s^2

I_{sp} = specific impulse; = $F/(\dot{m}g)$, s

J = current, A

$\dot{m}$ = propellant mass flow rate, kg/s

m_i = ion mass, kg

P = discharge power; = $J_d V_d$, W

r, z = cylindrical coordinates

R = inner radius, m

S_{out} = cross-sectional area of the discharge channel exit, m^2

V = voltage, V

η = thrust efficiency; = $F^2/(2\dot{m}JV)$

Subscripts

a = anode

c = cathode

d = discharge between anode and cathode

---

[1] Research Associate, Department of Aerospace Engineering
[2] Graduate Student, Department of Aerospace Engineering
[3] Associate Professor, Department of Aerospace Engineering
[4] Professor, Department of Aerospace Engineering, Associate Fellow AIAA

k = discharge between keeper and cathode

I. Introduction

GENERALLY, the outer surface of a satellite is equipped with a propulsion system. The available thrust is proportional to the product of satellite surface area and thrust density, whereas the satellite weight to the satellite volume. Based on the "square-cube law," larger satellites for orbit riding in all-electric satellite [1], space-debris removal, [2] or Mars cargo/piloted-class missions [3] require a higher thrust density because the short travel time is prioritized, and a smaller thrust density requires more time to attain a certain velocity increment. Therefore, thrust density is one of the most important factors [4] to reduce the propulsion system mass as much as possible [5]. A majority of the practical electric propulsion systems, such as ion thrusters and Hall thrusters, adopt the electrostatic acceleration method. Although the electrostatic thrust density is proportional to propellant mass flux, the suppliable propellant mass flux has limitations. In the ion thrusters, the thrust density is physically limited by Child–Langmuir law [6]. The Hall thrusters can avoid this limitation; however, there is an empirical limitation because of violent plasma instabilities and ensuring collision-less electrostatic ion acceleration. Dannenmayer et al [7] suggested an optimum propellant mass flux that a smaller mass flux leads to insufficient propellant ionization, and a larger mass flux leads to deteriorate thrust efficiency because of excessive electron cross-field transport by collisions. For decoupling the propellant ionization and acceleration, a double stage Hall thruster that has an inductively coupled plasma source between the anode and cathode was proposed [8]. The preliminary experimental results suggest that the expected thrust density was half that of the conventional Hall thrusters and the estimated thrust efficiency deteriorated as increasing the plasma source power. In contrast, magnetoplasmadynamic (MPD) thrusters are a reasonable alternative owing to their high thrust density because the electromagnetic acceleration has a collisional momentum transfer mechanism between ions and electrons [9]. The significant technical problems in the MPD thrusters are cathode erosion due to the large discharge current (which is of the order of 10^2 A) and lower thrust efficiency. Therefore, several challenges need to be overcome to improve the thrust density without deteriorating the thrust efficiency. Sasoh et al [10] proposed another type of ion acceleration method called electrostatic-magnetic hybrid ion acceleration. The thruster comprises a diverging magnetic field between a central cathode and a coaxially set ring anode. In this method, the ions generated near the anode experience both electrostatic acceleration and swirl acceleration through momentum transfer collision with electrons accelerated by the azimuthal Lorentz force. In this

Note, we present an operation characteristic of the hybrid ion acceleration method with supplying a high propellant mass flux. The obtained thrust density was higher than that of the purely electrostatic or electromagnetic acceleration method, and even with increasing discharge voltage, the violent plasma oscillation was not observed.

II. Experimental Setup

A. Thruster Head

Figure 1 schematically illustrates the thruster head developed in this study, which shares features with the thrusters referred to in Ref [11]; it has a cathode on the central axis and a ring anode placed coaxially around the cathode. A magnetic field was applied between the anode and cathode. The magnet was made of Sm-Co and has an inner diameter of 45 mm, an outer diameter of 100 mm, and a length of 30 mm. At the front and back surfaces of the magnet, magnetic yokes made of soft iron were mounted to strengthen the magnetic field (particularly near the anode) to enhance the near-anode ionization [12]. The ring anode was made of copper; its inner radius is denoted by R_a. It also had an inner surface that was tilted roughly relative to the magnetic lines of force. A commercial hollow cathode tip (LHC-03-AE1-01; Kaufman & Robinson, Inc.) with an in-built keeper electrode and insulating block was placed inside the anode. The propellant was fed through a 1.5-mm slit between the inner surface of the anode and the insulating block. The cylindrical coordinates (z, r) (where z and r are the axial and radial coordinates, respectively) were defined according to an axisymmetric configuration, with their origin located at the exit plane of the keeper electrode. At z = 20 mm (the thruster exit plane), the cross-sectional area at the thruster exit (S_{out}) was 1.0×10^{-3} m^2.

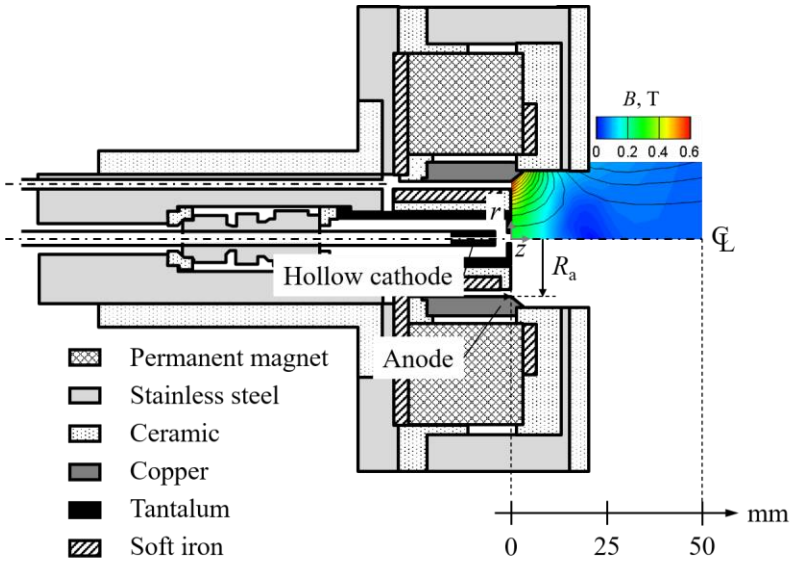

Fig. 1 Schematic of the thruster head and the applied magnetic field.

B. Vacuum Facility, Supply Equipment, and Thrust Measurement

In this section, we briefly describe the experimental environments of the vacuum facility, current and propellant supply systems, and thrust measurement system. The equipment details are described in our previous report [11]. All experiments were conducted in a stainless steel (ISO: 4301-304-00-I) vacuum chamber with an inner diameter of 1.2 m and a length of 3.2 m. The vacuum chamber was evacuated using a cryopump (pumping speed of 8400 L/s), which was backed up by a dry pump (pumping speed of 120 L/s). The base pressure of the system was 6.0×10^{-4} Pa. During system operation, a xenon (Xe) flow of 1.8–6.6 mg/s resulted in a chamber pressure of 1.1×10^{-2} – 2.9×10^{-2} Pa. Commercially available power supplies and mass flow control systems were used.

A pendulum-type thrust stand with a two-knife-edge fulcrum was used to measure the thrust directly. The displacement of the pendulum was measured using a laser displacement sensor (IL-S025; Keyence Co.) at the tip of the aluminum extension arm. The calibration factor was 305 mN/V for a range of up to 56 mN and an uncertainty of 0.2 mN. The measured "tare force" (an apparent thrust that should be corrected in the thrust measurement) was less than the thrust uncertainty and, therefore, ignored in this study.

III. Experimental Results and Discussions

A. Operation Conditions

The operation conditions are listed in Table 1. Regardless of R_a values, the anode inner angle was fixed at 45°, and B_c, $\dot{m}_c$, and J_k were set to 0.27 T, 0.49 mg/s, and 2.0 A, respectively. The maximum values of $\dot{m}_a$ and V_d were limited by the pumping capability of the vacuum system and specifications of commercial electrical feedthroughs, respectively. The purity of the gas was 99.995 %. The uncertainties in $\dot{m}_a$, V_d, and J_d were ± 0.1 mg/s, ± 2.0 V, and ± 51 mA, respectively. Experiments under each set of operation conditions were repeated minimum two times. Symbols represent the averaged value of each operation condition in the following figures, and error bars represent the standard deviation ($\pm\sigma$) obtained after several trials. Table 1 also summarized J_d, P_a, F, I_{sp}, and η_a with different R_a values. Among the operation conditions. both the maximum thrust (71 mN) and the highest thrust performances (1470 s of I_{sp} and 18% of η_a) were obtained in R_a = 15 mm with 2.7 kW of P_a. In terms of the mass penalty by applying the strengthened magnetic field, the thruster weight (5.5 kg) and maximum input power (2.7 kW) signifies a thruster weight-to-input power ratio of 2.0 kg/kW, which is comparative to that of the typical Hall thruster, 2.4 kg/kW [5].

Table 1 Operation conditions

R_a mm	$\dot{m}_a$ mg/s	V_d V	B_a T	J_d A	P_a kW	F mN	I_{sp} s	η_a %
9.0	1.3 – 4.1	100 – 325	0.43	1.7 - 7.4	0.1 - 1.3	5.3 - 30	396 - 1283	8.1 - 13
10.5	1.3 – 2.7	100 – 300	0.51	0.9 - 2.1	0.1 - 0.6	3.5 - 13	195 - 478	3.1 - 5.2
12.0	1.3 – 2.7	100 – 325	0.55	1.0 - 2.7	0.13 - 0.87	6.2 - 20	285 - 738	5.7 - 10
13.5	1.3 – 4.8	150 – 325	0.60	1.8 - 7.5	0.27 - 1.6	9.7 - 44	723 - 1376	10 - 17
15.0	2.0 – 6.1	200 – 500	0.59	2.3 - 9.8	0.66 - 2.7	17 - 71	850 - 1470	11 - 18

B. Electrostatic–Magnetic Hybrid Plasma Acceleration Characteristics

Figures 2 (a) and (b) illustrate the mass-averaged exhaust velocities $F/\dot{m}_a$ as a function of the characteristic velocity of electrostatic acceleration ($(2eV_d/m_i)^{½}$) and electromagnetic acceleration ($J_dB_cR_a/\dot{m}_a$), respectively. According to Fig. 2 (a), $F/\dot{m}_a$ was roughly linearly proportional to $(2\,eV_d/m_i)^{½}$ for all values of R_a. The maximum value of $F/\dot{m}_a$ was 14.4 km/s for R_a = 15.0 mm, which corresponds to a specific impulse of 1468 s. The factor of proportionality (α') depended on R_a; for R_a = 9.0 mm, 13.5 mm, and 15.0 mm, it exhibited similar levels in $0.4 \leq \alpha' \leq 0.6$, whereas α' was 0.3 and 0.2 for R_a values of 12.0 mm and 10.5 mm, respectively. The value of α' represents sources of momentum loss in the electrostatic acceleration process, such as a lower effective voltage for ion acceleration, insufficient ionization, and a large diverging half-angle. Therefore, R_a strongly affects the electrostatic acceleration performance.

Figure 2 (b) shows how the characteristic velocity of electromagnetic acceleration ($J_dB_cR_a/\dot{m}_a$) depends on $F/\dot{m}_a$ for different values of R_a. Regardless of the R_a value, $F/\dot{m}_a$ increased with increasing $J_dB_cR_a/\dot{m}_a$. For applied-field electromagnetic acceleration, the thrust can be represented as $F = \alpha J_dB_cR_a$ [10]. Fradkin et al. [13] assumed plasma in a hollow cylinder with inner and outer radii of R_c and R_a. respectively, which acted as a rigid rotator, in which the angular velocity is kept uniform at an axial location, and the rotational kinetic energy is fully converted to the axial kinetic energy after expansion through a diverging magnetic nozzle. In this model, an azimuthal torque is generated due to a Lorentz force induced by the interaction between $\mathbf{J_d}$ and $\mathbf{B_c}$ both of which have only (z, r) component. Under these assumptions, the thrust is given in a closed form as;

$$F = \frac{1}{\sqrt{2}} J_d B_a R_a \frac{1-\left(R_c/R_a\right)^2}{\sqrt{1+\left(R_c/R_a\right)^2}} \simeq \frac{1}{\sqrt{2}} J_d B_a R_a \left\{1-\frac{3}{2}\left(\frac{R_c}{R_a}\right)^2\right\} \tag{1}$$

In our experiment, $(R_c/R_a)^2 \sim 0.0025 << 1.0$, and we obtained $\alpha = 2^{-½}$. However, the experimentally obtained α, which is represented by the slope in Fig. 2 (b), exceeded this value and reached a maximum value of 2.5 for R_a = 15.0 mm. This high value of α requires a different acceleration mechanism because $F/\dot{m}_a$ is proportional to both $(2eV_d/m_i)^{½}$ and $J_dB_cR_a/\dot{m}_a$. Therefore, the experimentally obtained thrust should be contributed from electrostatic and electromagnetic

accelerations, namely electrostatic–magnetic hybrid plasma acceleration [10]. The presented α values were higher than that in our previous report ($\alpha \sim 2^{-½}$) [10]. There are two possible reasons for this increment; one is the enhanced-propellant ionization near anode and, consequently, increment in ion beam energy by strengthened magnetic field on anode because the ions fully utilize the potential drop between electrodes [12]. Another reason is that the multi-charged ions generate a larger thrust than the singly-charged ions because the electrostatic thrust is proportional to square-root of the charge-state. The discharge voltage (≥ 100 V) well exceeded the xenon-propellant ionization voltage (12.1 V and 21.2 V for singly- and doubly-ionization, respectively [14]), and both factors contributed to increase α. To breakdown the contributions from the two factors, ion beam characteristics (propellant utilization and current fractions from each charge-state ion) must be further investigated.

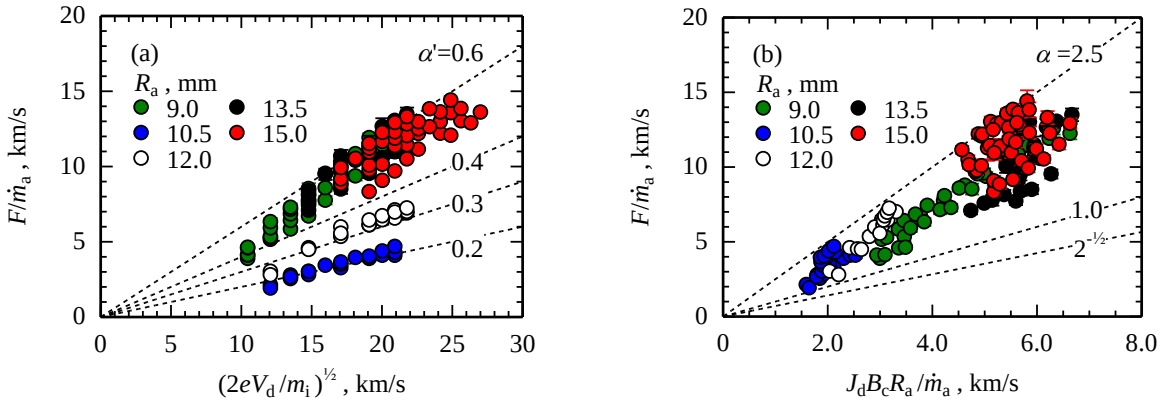

Fig. 2 Characteristic velocity vs $F/\dot{m}_a$ with different R_a (a) dependency on $(2eV_d/m_i)^{½}$, (b) dependency on $J_dB_cR_a/\dot{m}_a$. Operation conditions are summarized in Table 1.

C. Comparison of Operation Characteristics with those of Hall Thruster

In this section, the operating characteristics obtained in this study (J_d, thrust density F/S_{out}, and $\eta_a \equiv F^2/(2\dot{m}_aJ_dV_d)$) are compared to those of typical Hall thrusters. The thrust performances observed in this study for different R_a values at V_d = 250 V are shown in Fig. 3. The horizontal axis represents the propellant mass flux $\dot{m}_a/S_{out}$, which ranged from 1.3×10^{-3} kg/(s·m^2) to 6.1×10^{-3} kg/(s·m^2). The current J_d increased with increasing $\dot{m}_a/S_{out}$. The maximum J_d was 9.8 A, which is much smaller than the conventional MPD thruster operating current (of the order of 10^2 A [9]) and less than the commercially ensured current of the cathode tip (20 A). Even with a small discharge current, electrostatic–magnetic hybrid acceleration was achieved. The thrust density F/S_{out} increased linearly with increasing $\dot{m}_a/S_{out}$ for $I_{sp,a} \equiv F/(\dot{m}_ag)$ values of 400 s (R_a = 10.5 mm), 600 s (R_a = 12.0 mm), and 1200 s (R_a = 9.0 mm, 13.5 mm, and 15.0 mm).

The maximum F/S_{out} was 70 N/m^2 for R_a = 15.0 mm. The efficiency η_a increased at first, and for $\dot{m}_a/S_{out} \geq 3.3\times10^{-3}$ kg/(s·m^2), η_a was maintained within 17 ± 1%. Because of the smaller J_d values, F/S_{out} and η_a for R_a = 10.5 mm and 12.0 mm were also smaller than those of other R_a settings.

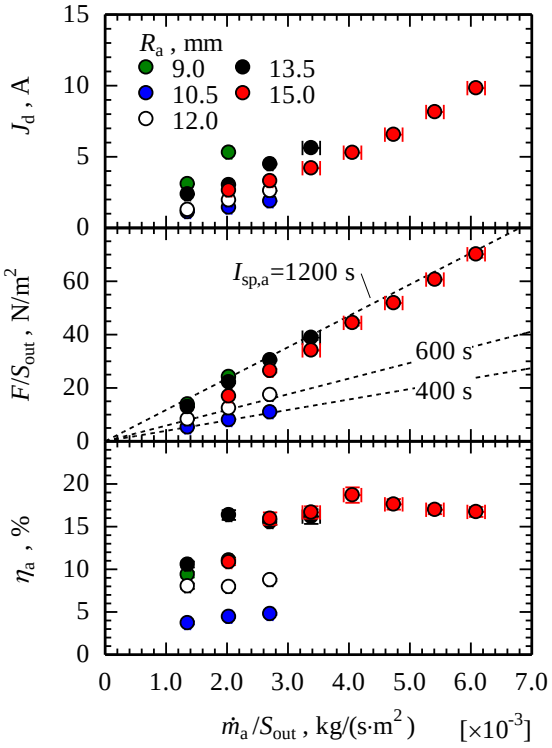

Fig. 3 $\dot{m}_a/S_{out}$ vs J_d, F/S_{out}, and η_a for different R_a, V_d = 250 V, S_{out} = 1.0×10^{-3} m^2.

Next, these values were compared to those of the Hall thruster. To estimate $\dot{m}_a/S_{out}$, F/S_{out}, η_a, and $I_{sp,a}$ for the typical Hall thruster, a scaling law derived from experimental results of 1-kW-class 18 Hall thrusters was used as a reference value [15]. In the Hall thruster operation, $\dot{m}_a/S_{out}$ should be 0.9×10^{-3} kg/(s·m^2) to ensure a stable plasma discharge and an efficient thruster operation. Because $\dot{m}_a/S_{out}$ is uniquely decided, F/S_{out} and $I_{sp,a}$ are proportional only to $(V_d)^{½}$. For the same $I_{sp,a}$ value (~1200 s), V_d, F/S_{out} and η_a were calculated as 174 V, 11 N/m^2, and 45%, respectively, using the coefficients of thruster geometry, mass flow rate, thrust, and discharge power. In this study, a stable operation was achieved for $\dot{m}_a/S_{out} \leq 6.1\times10^{-3}$ kg/(s·m^2), and a decrement in η_a was not observed. Owing to this high mass flux, the thrust density increased up to 6.3 times higher than the scaled value for Hall thrusters. In terms of the multi-mode (large thrust/high specific impulse) operation [1], the high-thrust-density operation would be useful for the large thrust mode. For high specific impulse mode [16], the violent plasma oscillations caused by neutral depression [17] was not

observed even with increased V_d. Therefore, the presented thruster also exhibited a capability for stable, high-specific-impulse operation. In spite of these advantages, however, the thrust efficiency should be improved. One possible approach is scaling up both thruster size and input power [18]. To inquire the reason for the lower thrust efficiency, a data set of both plasma parameters (electron number density, temperature, and space potential distributions) and efficiencies (propellant/current utilization, beam energy, and beam divergence) are required, which is beyond the scope of this study and warrants further investigations.

IV. Conclusions

We investigated operation characteristics of an electrostatic-magnetic hybrid ion acceleration method under a diverging magnetic field. The obtained mass-averaged exhaust velocity exhibited dual aspects of the electrostatic and electromagnetic characteristic velocities, namely electrostatic-magnetic hybrid ion acceleration. The measured thrust was higher (by a factor of 2.5) than the electromagnetic thrust for a discharge current of less than 10 A, which is the practical current level for hollow cathode electron emissions. By increasing the propellant mass flux, the thrust density increased up to 70 N/m^2 without violent plasma oscillations. Compared to a scaled model of Hall thrusters, the thrust density was higher by a factor of 6.3 at identical specific impulse of 1200 s. However, the results of lower thrust efficiency (up to 18 %) warrants further investigations of both plasma parameters and ion beam characteristics.

Acknowledgments

This study was supported by the Japan Society for the Promotion of Science (JSPS) KAKENHI 18H03813.

References

[1] Funaki, I., Cho, S., Sano, T., Fukatsu, T., Tashiro, Y., Shiiki, T., Nakamura, Y., Watanabe, H., Kubota, K., Matsunaga, Y., and Fuchigami, K., "Development of a 6-kW-class Hall thruster for geostationary missions," *Acta Astronautica* Vol. 170, 2020, pp. 163-171.
https://doi.org/10.1016/j.actaastro.2019.08.029

[2] Takahashi, K., Charles, C., Boswell, R. B., and Ando, A., "Demonstrating a new technology for space debris removal using a bidirectional plasma thruster," *Scientific Reports* Vol. 8, 2018, Paper 14417.
https://doi.org/10.1038/s41598-018-32697-4

[3] Sankaran, K., Cassady, L., Kodys, A. D., and Choueiri, E. Y., "A Survey of Propulsion Options for Cargo and Piloted Missions to Mars," *Annals of the New York Academy of Sciences,* Vol. 1017, 2004, pp. 450–467. https://doi.org/10.1196/annals.1311.027

[4] Krülle, G., Kurtz, M. A., and Akihiro, S., "Technology and Application Aspects of Applied Field Magnetoplasmadynamic Propulsion," *Journal of Propulsion and Power,* Vol. 14, No. 5, 1998, pp. 754–763. https://doi.org/10.2514/2.5338

[5] Hofer, R. R., and Randolph, T. M., "Mass and Cost Model for Selecting Thruster Size in Electric Propulsion Systems," *Journal of Propulsion and Power,* Vol. 29, No. 1, 2013, pp. 166–177. https://doi.org/10.2514/1.B34525

[6] Chen, F., F., *Introduction to Plasma Physics and Controlled Fusion* 2nd ed., Plenum Press, New York, 1984, Sec. 8.2.4. https://doi.org/10.1007/978-3-319-22309-4

[7] Dannenmayer, K., and Mazouffre, S., "Elementary Scaling Relations for Hall Effect Thrusters," *Journal of Propulsion and Power,* Vol. 27, No. 1, 2011, pp. 236–245. https://doi.org/10.2514/1.48382

[8] Martin, A., O., Guglieimi, A., Gaboriau, F., Boniface, C., and Bouef, J., P., "Experimental characterization of ID-Hall, a double stage Hall thruster with an inductive ionization stage," *Physics of Plasmas* Vol. 27, No. 2, 2020, Paper 023518. https://doi.org/10.1063/1.5140241

[9] Sasoh, A. and Arakawa, Y., "Electromagnetic Effects in an Applied-Field Magnetoplasmadynamic Thruster," *Journal of Propulsion and Power,* Vol. 8, No. 1, 1992, pp. 98–102. https://doi.org/10.2514/3.23448

[10] Sasoh, A., Mizutani, K., and Iwakawa, A., "Electrostatic/magnetic ion acceleration through a slowly diverging magnetic nozzle between a ring anode and an on-axis hollow cathode," *AIP Advances,* Vo. 7, No. 6, 2017, Paper 065204. https://doi.org/10.1063/1.4985380

[11] Ichihara, D., Nakagawa Y., Iwakawa A., and Sasoh, A., "Central and External Cathode Operations in a Diverging-Magnetic-Field Electrostatic Thruster," *Journal of Propulsion and Power,* Vol. 36, No. 1, 2020, pp. 68-77. https://doi.org/10.2514/1.B37636

[12] Ichihara, D., Iwakawa, A., and Sasoh, A., "Effects of Magnetic Field Profile near Anode on Ion Acceleration Characteristics of a Diverging Magnetic Field Electrostatic Thruster," *Journal of Applied Physics,* Vol. 122, No. 4, 2017, Paper 043302. https://doi.org/10.1063/1.4995286

[13] Fradkin, D. B., Blackstock, A. W., Roehling, D. J., Stratton, T. F., Williams, M., and Liewer, K.W., "Experiments Using a 25-kW Hollow Cathode Lithium Vapor MPD Arcjet," *AIAA Journal,* Vol. 8, No. 5, 1970, pp. 886–894.

https://doi.org/10.2514/3.5783

[14] Sorokin, A. A., Shamenok, L. A., Bobashev, S. V., Möbus, B., Richter, M., and Ulm, G., "Measurements of electron-impact ionization cross sections of argon, krypton, and xenon by comparison with photoionization," *Physical Review A*. Vol. 61, 2000, Paper 022723.
https://doi.org/10.1103/PhysRevA.61.022723

[15] Lee E., Kim Y., Lee H., Kim H, Doh G., Lee D., and Choe W., "Scaling Approach for Sub-Kilowatt Hall-Effect Thrusters," *Journal of Propulsion and Power*, Vol. 35, No. 6, 2019, pp. 1073-1079.
https://doi.org/10.2514/1.B37424

[16] Hofer, R. R., Jankovsky, R. S., and Gallimore, A. D., "High-Specific Impulse Hall Thrusters, Part 1: Influence of Current Density and Magnetic Field," *Journal of Propulsion and Power*, Vol. 22, No. 4, 2006, pp. 721-731.
https://doi.org/10.2514/1.15952

[17] Giannetti, V., Saravia, M. M., and Andreussi, T., "Measurement of the breathing mode oscillations in Hall thruster plasmas with a fast-diving triple Langmuir probe," *Physics of Plasmas*, Vol. 27, 2020, Paper 123502.
https://doi.org/10.1063/5.0022928

[18] Conversano, R., W., Goebel, D. M., Hofer, R. R., Mikellides, G., Wirz, R. E., "Performance Analysis of a Low-Power Magnetically Shielded Hall Thruster: Experiments," *Journal of Propulsion and Power*, Vol. 33, No. 4, 2017, pp. 975-983.
https://doi.org/10.2514/1.B34525